Chaotic electron dynamics in gyrotron resonators

Y. Kominis
School of Electrical and Computer Engineering, National Technical University of Athens, Association EURATOM-Hellenic Republic, Zographou GR-15773, Greece

O. Dumbrajs
Department of Engineering Physics and Mathematics, Helsinki University of Technology, Association EURATOM-TEKES, FIN-02150 Espoo, Finland

K. A. Avramides, K. Hizanidis, and J. L. Vomvoridis
School of Electrical and Computer Engineering, National Technical University of Athens, Association EURATOM-Hellenic Republic, Zographou GR-15773, Greece

(Received 19 October 2004; accepted 11 January 2005; published online 16 March 2005)

Phase space analysis of electron dynamics is used in combination with the canonical perturbation method and the KAM (Kolmogorov–Arnold–Moser) theory in order to study the dependence of the efficient gyrotron operation on the rf field profile and frequency mismatch. Knowledge of the boundaries of the electron motion provided through robust (slightly distorted) KAM surfaces is useful for optimizing depressed collectors and thereby for enhancement of overall efficiency of gyrotron operation. © *2005 American Institute of Physics*. [DOI: 10.1063/1.1867496]

I. INTRODUCTION

A gyrotron is an important source of the short wavelength coherent radiation whose operation is based on the stimulated cyclotron radiation of electrons oscillating in a static magnetic field and interacting with a rf field in the gyrotron cavity. High power gyrotrons in the millimeter wave range are developed worldwide for the electron cyclotron heating of the plasma in nuclear fusion installations[1–3] and for technological applications.[4] The physics of gyrotrons has been presented in details in a new monograph.[5] One of the interesting and important aspects of this physics is understanding of stochastic processes in gyrotrons (see Ref. 6, and references therein). Three types of stochasticity should be distinguished. (i) Electron residual energies can become stochastic after interaction with the rf field in a resonator and complicate efficient operation of depressed collectors. (ii) stochastic rf oscillations can appear when electron beam current exceeds certain threshold values that are dependent on other operating parameters. This leads to a dramatic decrease in efficiency and the appearance of other frequencies in the output signal in addition to the desired one. (iii) Spatiotemporal chaos in the rf field structure can show up in a large-diameter cavities when modes with high azimuthal indices are used. Here (ii) has received the most study both theoretical and experimental, while (i) and (iii) can be regarded as relatively unexplored parts of the stochastic phenomena in gyrotrons.

In this work we continue investigations of chaotic electron dynamics in gyrotron resonators. The mechanism of radiation emission is directly connected with the electron dynamics inside the cavity, which are described by a nonlinear dynamical system. The latter is nonintegrable and it possesses the characteristic features of complex dynamics such as inhomogeneity of the phase space and strong dependence on the initial conditions. Although complex systems and more specifically wave–particle interactions have been studied extensively in the scientific literature,[7] only periodic waves have been considered. However, in the case of a gyrotron oscillator, the geometry of the cavity results in an aperiodic rf field profile, and the electron dynamics are governed by an aperiodically perturbed Hamiltonian system.[8–10]

We apply a canonical perturbation method in order to construct analytically approximate invariants of the electron motion corresponding to KAM (Kolmogorov–Arnold–Moser) surfaces,[7] which contain all the essential information of the phase space structure of the dynamical system. Phase space analysis provides useful results for parameter selection for high efficiency gyrotron operation as well as preliminary information for the electron rest energies which is essential for the design and optimization of depressed collectors[11] which are widely used in vacuum microwave tubes for enhancement of overall efficiency. Of course, the efficient design and use of depressed collectors requires accurate knowledge of distribution of the electron rest energies in the context of the self-consistent model of wave–particle interaction, while stochasticity suggests that the residual energies of part of the electrons cannot be predicted.

II. PHYSICAL MODEL

The simplest equation which describes the electron motion in a gyrotron resonator have been derived by Yulpatov (see details in Ref. 5):

$$\frac{dp}{d\zeta} + i(\Delta + |p|^2 - 1)p = iFf(\zeta) \tag{1}$$

with the initial condition $p(\zeta_0)=\exp(i\theta_0)$, $0 \leqslant \theta_0 \leqslant 2\pi$. Here, p is the dimensionless transverse momentum of the electron, $\zeta=(\beta_{\perp 0}^2\omega/2\beta_{\|0}c)z$ is the dimensionless coordinate, $\beta_{\perp 0}=v_{\perp 0}/c$ and $\beta_{\|0}=v_{\|0}/c$ are the normalized transverse and parallel velocities of the electron at the entrance to the cavity, $\Delta=2(\omega-\omega_c)/\beta_{\perp 0}^2\omega$ is the frequency mismatch, $\omega_c=(e/m)B/\gamma_{rel}$ is the electron cyclotron frequency, B is the

magnetic field in tesla, $\gamma_{rel}=1+(mc^2/e)^{-1}U$ is the relativistic factor, U is the accelerating voltage, and F is the dimensionless beam to rf coupling factor.

The differential equation (1) represents the cold-cavity approximation when the rf field $f(\zeta)$ depends only on the geometry of the resonator, but not on the electron motion (f does not depend on p). In this case the rf field can be approximated by a Gaussian

$$f(\zeta)=\exp\left[-\left(\frac{2\zeta}{\mu}-\sqrt{3}\right)^2\right], \tag{2}$$

where $\mu=\pi(\beta_{\perp 0}^2/\beta_{\|0})L/\lambda$ is the dimensionless length of the resonator with length L. The aforementioned approximation is valid in resonators with very high quality factors.[12] By considering the complex p in its Cartesian form $p=Q+iP$ the Eq. (1) is transformed to the following system of coupled differential equations:

$$\begin{aligned}\frac{dQ}{d\zeta}&=-\delta P+P(Q^2+P^2)-Fg(\zeta),\\ \frac{dP}{d\zeta}&=+\delta Q-Q(Q^2+P^2)+Fh(\zeta),\end{aligned} \tag{3}$$

where $\delta=1-\Delta$, $h(\zeta)=\mathrm{Re}[f(\zeta)]$, $g(\zeta)=\mathrm{Im}[f(\zeta)]$.

III. HAMILTONIAN FORMULATION

The set of Eqs. (3) represents a one degree of freedom, nonautonomous Hamiltonian system (the dimensionless position coordinate ζ can be regarded as time), with the Hamiltonian

$$H(Q,P,\zeta;F)=-\frac{\delta}{2}(Q^2+P^2)+\frac{1}{4}(Q^2+P^2)^2-F[Qh(\zeta)+Pg(\zeta)]. \tag{4}$$

The system (3) can be considered as a autonomous system in the extended phase space $(P,-H,Q,\zeta)$ where $-H$ and ζ are treated as momentum and coordinate in a four-dimensional phase space (two degree of freedom system). The flow is parametrized by new "time" t and the new Hamiltonian has the form $\bar{H}(P,-H,Q,\zeta)=H(P,Q,\zeta)-H$.[7] The new Hamiltonian $\bar{H}$ does not depend explicitly on the new time t and thus, it is a constant of the motion. However, the existence of a second constant of the motion is required so that the system is integrable, but this is not expected in the general case. Only a few special rf field profiles $f(\zeta)$ result in the existence of a second constant of the motion, such as $f(z)=\exp(ik\zeta)$,[8] so that in general the system is considered as nonintegrable.

IV. THE UNPERTURBED (INTEGRABLE) SYSTEM

In order to study a nonintegrable system we can start from an integrable system which differs from the actual one in terms of a small parameter and consider the actual system as a perturbation of the integrable one (near integrable). In our case the unperturbed (integrable) system can be defined as the one which describes the electron motion in the absence of the rf field with Hamiltonian

$$H_0(P,Q)=H(P,Q,\zeta;F=0)=-\frac{\delta}{2}(Q^2+P^2)+\frac{1}{4}(Q^2+P^2)^2. \tag{5}$$

For this system, the Hamiltonian H_0 does not depend explicitly on time, and represents the conserved energy of the electrons under no interaction with a rf field. The Hamiltonian of the perturbed system can be written in the following form:

$$H(P,Q,\zeta;F)=H_0(P,Q)+H_1(P,Q,\zeta;F), \tag{6}$$

where $H_1(P,Q,\zeta;F)=-F[Qh(\zeta)+Pg(\zeta)]$ is the perturbative term representing the presence of the rf field. The coupling factor F can be considered as the small parameter in the perturbation approach which follows. From a physical point of view a small F is required in order to preserve the gyrating character of the electron motion.

Starting from the unperturbed system, we transform the original variables (P,Q) to action-angle variables (J,θ),

$$\begin{aligned}J&=\frac{P^2+Q^2}{2},\\ \theta&=\arcsin\left(\frac{Q}{\sqrt{P^2+Q^2}}\right).\end{aligned} \tag{7}$$

The transformed Hamiltonian has the form

$$H_0(J)=J^2-\delta J \tag{8}$$

leading to the following system of equations of the motion:

$$\begin{aligned}\frac{dJ}{d\zeta}&=0,\\ \frac{d\theta}{d\zeta}&=\omega_\theta,\end{aligned} \tag{9}$$

where

$$\omega_\theta=\frac{\partial H_0(J)}{\partial J}=2J-\delta. \tag{10}$$

V. THE PERTURBED (NEAR-INTEGRABLE) SYSTEM

The Hamiltonian of the perturbed (near-integrable) system can be written in terms of the action-angle variables of the unperturbed system as follows:

$$H(J,\theta,\zeta;F)=H_0(J)+H_1(J,\theta,\zeta;F), \tag{11}$$

where $H_0(J)$ is given in Eq. (8) and

$$H_1(J,\theta,\zeta;F)=F\sqrt{2J}[h(\zeta)\sin(\theta)+g(\zeta)\cos(\theta)] \tag{12}$$

or

$$H_1(J,\theta,\zeta;F)=F\sqrt{2J}\,\mathrm{Im}\{\exp(i\theta)f(\zeta)\}. \tag{13}$$

At this point we must emphasize that the aperiodic dependence of the perturbation term on the time ζ differentiates the topology of the flow in the extended phase space: instead of the usual tori $[(J,\theta,\zeta)\in\mathbb{R}\times\mathbb{T}^2]$ resulting from time-periodic perturbations, we deal with infinite cylinders

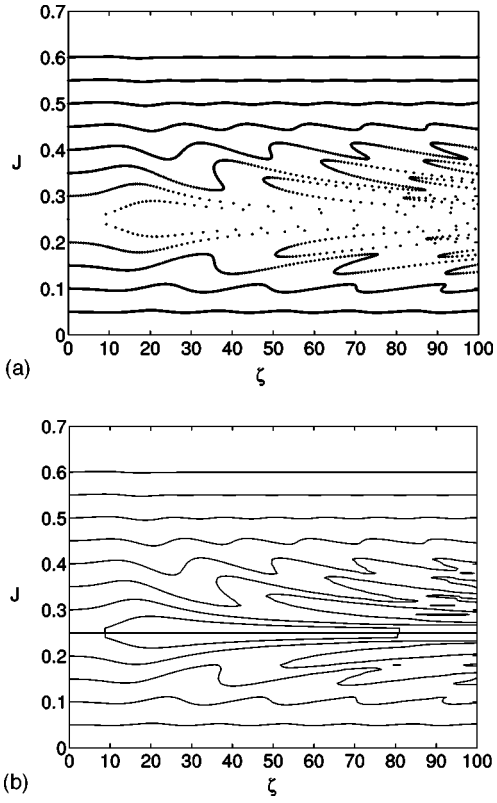

FIG. 1. (a) Numerically and (b) analytically obtained Poincaré surface of section for $F=0.005$, $\Delta=0.5$, and $\mu=15$.

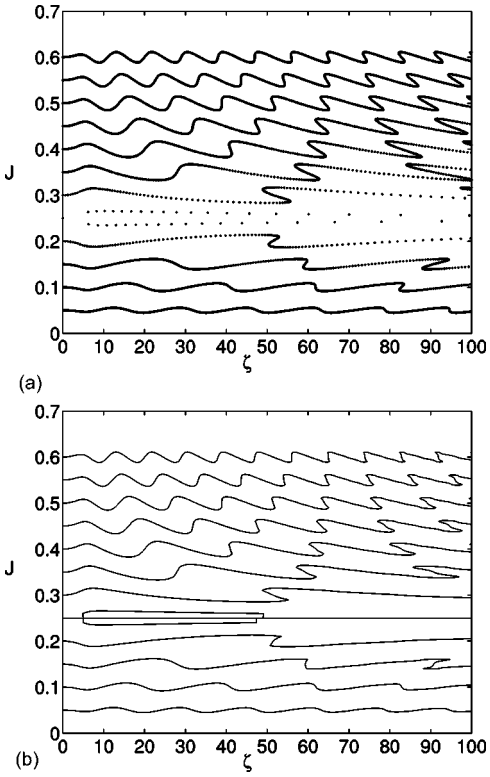

FIG. 2. (a) Numerically and (b) analytically obtained Poincaré surface of section for $F=0.005$, $\Delta=0.5$, and $\mu=5$.

$[(J,\theta,\zeta)\in\mathbb{R}\times\mathbb{T}\times\mathbb{R}]$. Major differences between the two configurations of the phase space have made the study of the aperiodic case a still interesting problem from the point of view of the dynamical systems analysis. The approximate construction of the corresponding KAM curves can be made by using the canonical perturbation theory.

As a prerequisite of the application of the KAM theory which holds for both the periodic and the aperiodic case the condition of nondegeneracy of the unperturbed Hamiltonian (also known as condition of sufficient nonlinearity) must hold, i.e.,

$$\frac{\partial^2 H_0(J)}{\partial J^2}\neq 0. \tag{14}$$

In order to construct the KAM curves of the perturbed system we use successively near-identity canonical transformations to transform the Hamiltonian to a normal form in which the θ and ζ dependence is pushed to higher order terms with respect to the small parameter of the perturbation method. The procedure can be continued to any order, resulting in series which converge to the actual KAM curves in specific regions in the phase space. However, as will be shown, even a first-order approximation is capable of providing accurate information about the structure of the phase space and the features of the flow.

Following a standard procedure,[7] we seek a transformation to new variables $(\bar{J},\bar{\theta})$ for which the new Hamiltonian $\bar{H}$ is a function of the action $\bar{J}$ alone. Using the generating function $S(\bar{J},\theta)$ we expand S and $\bar{H}$ in power series of a small parameter ϵ (in our case $\epsilon\equiv F$)

$$S=\bar{J}\theta+\epsilon S_1+\cdots, \tag{15}$$

$$\bar{H}=\bar{H}_0+\epsilon\bar{H}_1+\cdots, \tag{16}$$

where the lowest-order term has been chosen to generate the identity transformation $J=\bar{J}$ and $\bar{\theta}=\theta$. The old action and angle can be also expressed as power series in ϵ:

$$J=\bar{J}+\epsilon\frac{\partial S_1(\bar{J},\theta,\zeta)}{\partial\theta}+\cdots, \tag{17}$$

$$\bar{\theta}=\theta+\epsilon\frac{\partial S_1(\bar{J},\theta,\zeta)}{\partial\bar{J}}+\cdots. \tag{18}$$

The new Hamiltonian is

$$\bar{H}(\bar{J},\bar{\theta},\zeta)=H(J,\theta,\zeta)+\frac{\partial S(\bar{J},\theta,\zeta)}{\partial\zeta}. \tag{19}$$

In order to find $\bar{H}$, Eqs. (17) and (18) must be inverted to give the old variables in terms of the new. To order ϵ this can be done easily:

$$J=\bar{J}+\epsilon\frac{\partial S_1(\bar{J},\bar{\theta},\zeta)}{\partial\bar{\theta}}+\cdots, \tag{20}$$

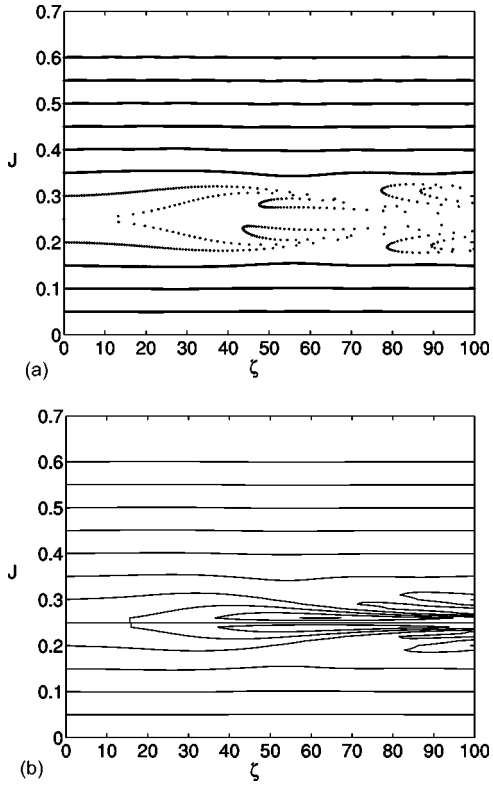

FIG. 3. (a) Numerically and (b) analytically obtained Poincaré surface of section for $F=0.005$, $\Delta=0.5$, and $\mu=45$.

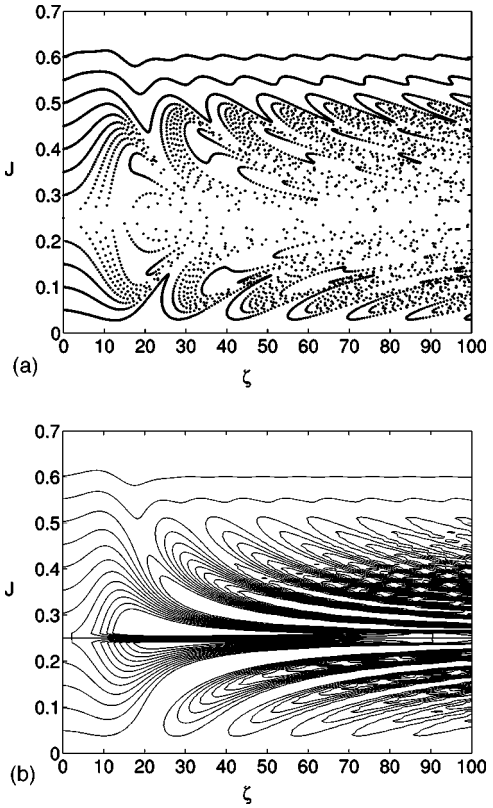

FIG. 4. (a) Numerically and (b) analytically obtained Poincaré surface of section for $F=0.05$, $\Delta=0.5$, and $\mu=15$.

$$\theta = \overline{\theta} - \epsilon \frac{\partial S_1(\overline{J}, \theta, \zeta)}{\partial \overline{J}} + \cdots . \tag{21}$$

Inserting these equations into Eq. (19) and equating like powers of ϵ, we have to zero order

$$\overline{H_0} = H_0(\overline{J}) \tag{22}$$

and to first order

$$\overline{H_1} = \frac{\partial S_1}{\partial \zeta} + \omega_\theta \frac{\partial S_1}{\partial \overline{\theta}} + H_1. \tag{23}$$

In order to eliminate the $\overline{\theta}$- and ζ-dependent part of H_1, S_1 must be chosen appropriately. Introducing the average (over both θ and ζ) part of H_1 as $\langle H_1 \rangle$ and the remaining part as $\{H_1\}=H_1-\langle H_1 \rangle$ we have the following equations:

$$\overline{H} = H_0 + \epsilon \langle H_1 \rangle \tag{24}$$

and

$$\frac{\partial S_1}{\partial \zeta} + \omega_\theta \frac{\partial S_1}{\partial \overline{\theta}} = -\{H_1\}. \tag{25}$$

For the specific perturbation considered (13) it is obvious that $\langle H_1 \rangle = 0$ and $\{H_1\}=H_1$. In order to solve the linear differential equation (25) to obtain S_1, instead of using the usual Fourier series method which apply for periodic perturbation, we use the Fourier transform method so that Eq. (25) transforms to

$$i\Omega \mathbb{S}_1 + \omega_\theta (ik) \mathbb{S}_1 = 2\pi F \sqrt{2J} \mathbb{F}(\Omega) \delta(k-1), \tag{26}$$

where $\theta \rightleftharpoons k$, $\zeta \rightleftharpoons \Omega$, and $\mathbb{S}_1(J,k,\Omega)$, $\mathbb{F}(\Omega)$ are the Fourier transforms of $S_1(J,\theta,\zeta)$ and $f(\zeta)$, respectively. Note that, for simplicity, we work with the complex equation, but we have to take only the imaginary part, according to Eq. (13), at the final results. Solving Eq. (26) and using the inverse Fourier transform, S_1 is obtained as follows:

$$S_1 = -iF\sqrt{2J} \exp(i\theta) \frac{1}{2\pi} \int_{-\infty}^{+\infty} \frac{\mathbb{F}(\Omega)}{\Omega + \omega_\theta} \exp(i\Omega z) d\Omega. \tag{27}$$

Defining

$$I_0[\omega_\theta(J), \zeta] = \frac{1}{2\pi} \int_{-\infty}^{+\infty} \frac{\mathbb{F}(\Omega)}{\Omega + \omega_\theta} \exp(i\Omega\zeta) d\Omega, \tag{28}$$

the new action is obtained from Eq. (17),

$$\overline{J} = J - F\sqrt{2J}\, \mathrm{Im}\{I_0 \exp(i\theta)\}. \tag{29}$$

The calculation of I_0 for an arbitrary rf profile $f(\zeta)$ is given in the Appendix. For the case of the Gaussian profile (2), we have

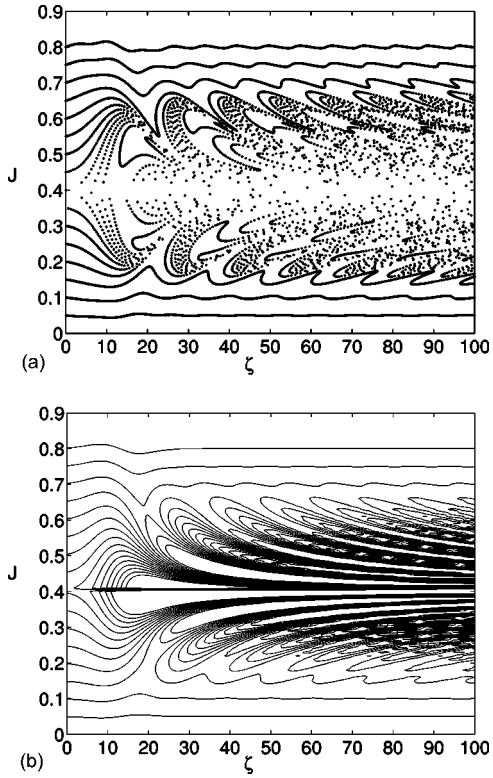

FIG. 5. (a) Numerically and (b) analytically obtained Poincaré surface of section for $F=0.05$, $\Delta=0.2$, and $\mu=15$.

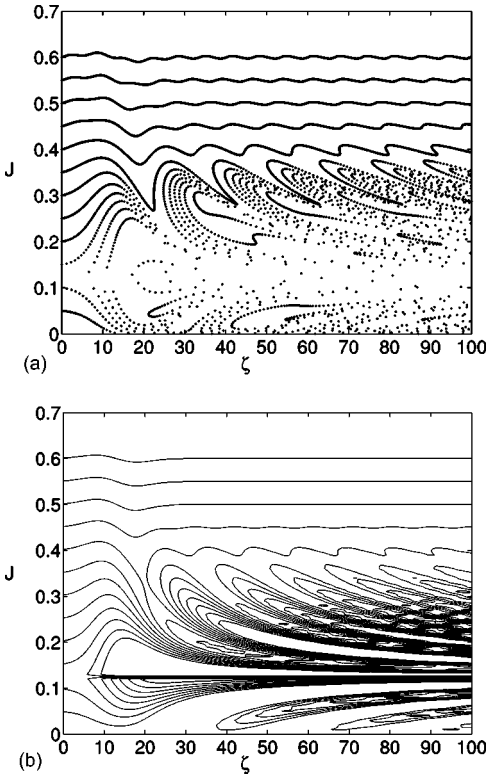

FIG. 6. (a) Numerically and (b) analytically obtained Poincaré surface of section for $F=0.05$, $\Delta=0.75$, and $\mu=15$.

$$I_0 = \sigma\sqrt{\frac{\pi}{2}}e^{-(\omega_\theta^2\sigma^2/2)}e^{-i\omega_\theta(\zeta-\zeta_0)} \times\left[1+\mathrm{erf}\left(\frac{(\zeta-\zeta_0)-i\omega_\theta\sigma^2}{\sqrt{2}\sigma}\right)\right] \tag{30}$$

where $\mathrm{erf}(x), x\in\mathbb{C}$ is the error function, $\sigma^2=\mu^2/8$ and $\zeta_0=\sqrt{3}\mu/2$.

VI. RESULTS AND DISCUSSION

In order to study the dynamics of the system governing the electron motion under the presence of a rf field we consider the phase space of the system, which we can be analyzed using appropriate Poincaré surfaces of section. As we have already mentioned, the extended phase space of the system is four dimensional. Since the Hamiltonian ($\bar{H}$) in the extended phase space is time independent, the flow can be considered in the three-dimensional space $\bar{H}=\text{const}$. Considering the unperturbed system in action-angle variables (8), the flow can be described by infinite cylinders of constant radius, which is given by the value of the action variable. According to the KAM theorem, some of these cylinders persist under small perturbations (small amplitude of the rf field), although the action is no longer a constant of the motion and the flow is not independent of the angle variable (loss of cylindrical symmetry). The new action (29), obtained by the canonical perturbation method, is a local approximate constant of the motion. Moreover, under strong perturbation there are "cylinders" of a specific radius range which can be destroyed, resulting in a significant change in the topology of electron trajectories. As will be shown, the latter is essential for the operation of gyrotrons in parameter ranges of high efficiency.

The topology of the KAM surfaces in the phase space can be described by using a Poincaré surface of section defined as follows:

$$\Sigma=\left\{(P,\zeta):Q=0,\frac{dQ}{d\zeta}>0\right\}. \tag{31}$$

The definition of the Poincaré surface of section in terms of the variables (Q,P) instead of the usual definition in terms of the action-angle variables ($\Sigma'=\{(J,\zeta):\theta=\text{const},d\theta/d\zeta>0\}$) has the advantage of tracking both clockwise and counterclockwise electron gyrations, which take place for $\delta>0$ and appropriate action values (10). The KAM curves can be constructed numerically but also analytically, as contour plots of the approximate local invariant (29) and contain all the essential features of the electron dynamics. In order to take appropriately into account both directions of gyrations we can set $\theta'=\theta+[\mathrm{sgn}(\omega_\theta)-1]\pi/2$ in (29) so that we can have the Poincaré surface of section (31) for $\theta=0$.

In the following figures (Figs. 1–8) several cases of Poincaré surfaces of section are shown, exhibiting the features of electron dynamics under a variety of rf field profiles (in terms of F and μ) and frequency mismatch Δ. The numerically obtained surfaces of section are constructed using initial conditions consisted of a range of values of actions J and uniformly distributed angles θ in the range $[0\ 2\pi)$ for each action value. However, since the transverse momentum of the electron p in Eq. (1) is normalized to unity, the action

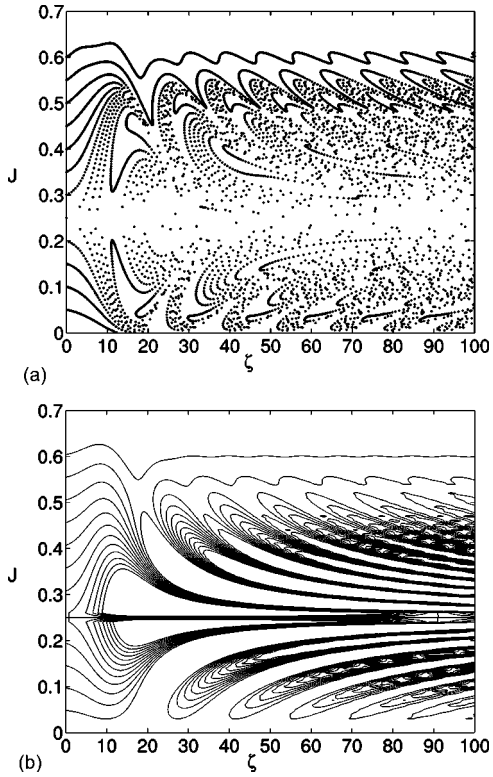

FIG. 7. (a) Numerically and (b) analytically obtained Poincaré surface of section for $F=0.1$, $\Delta=0.5$, and $\mu=15$.

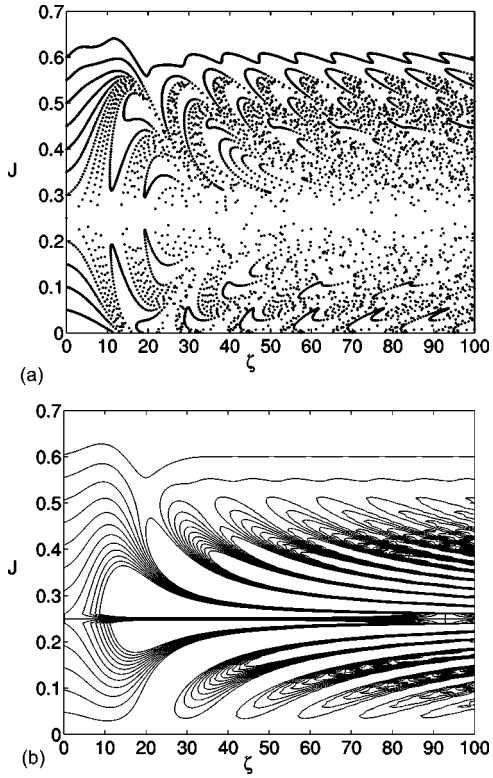

FIG. 8. (a) Numerically and (b) analytically obtained Poincaré surface of section for $F=0.125$, $\Delta=0.5$, and $\mu=17$ (maximum efficiency $n_{\perp}=0.71$).

value $J=0.5$ is of particular interest for the gyrotron operation. For all cases there exists an area of drastic interactions around $J_0=\delta/2$, which is the boundary action value between areas of opposite direction of rotation (10) with respect to the frame of the rf field, for the unperturbed system.

In Fig. 1 the case of a rf field profile having $F=0.005$, $\mu=15$, and a frequency mismatch $\Delta=0.5$ is shown. The KAM surfaces bounding the flow in the phase space are close to cylinders for action values sufficiently far from J_0. Action values close to J_0 result in electron motion which is no longer bounded in a cylindrical surface: a drastic modification of the topology of electron trajectories is manifested as a destruction of the corresponding KAM curves. The inhomogeneous (in action) character of this destruction implies the existence of a resonance between the continuous spectrum of the rf field and the action-dependent frequencies of the unperturbed electron motion: since the spectral component of the rf field for the Gaussian profile (2) with highest amplitude is $\Omega=0$, the action value J_0 corresponds to a 1-1 resonance. In our analytical approximation of the KAM curves, this resonant modification is expressed through the denominator of the integrand in Eq. (28). It is remarkable that, the presence of multiple rf modes and the corresponding existence of multiple resonant regions can lead to increased stochasticity of electron trajectories under conditions which result in resonant regions overlap in a way similar to what is shown in Ref. 10. However, this investigation as well as the correlation between the stochasticity of electron trajectories and the rf field profile goes beyond the scope of this work where we focus on the dependency of the width and the position of a single resonant region on the operation parameters.

The effect of the dimensionless resonator length on the electron motion is shown in Figs. 2 and 3, for a smaller and a larger value of μ, respectively. It is obvious that μ determines the width of the strong interaction area around J_0, for a given F: A small μ describes a short rf profile in ζ, which has a more spread frequency spectrum and consequently can resonate with a greater range of electron frequencies (and actions), while the opposite holds for a large μ. It is remarkable that for the aforementioned cases the analytically obtained approximate invariants are in both qualitative and quantitative agreement with the numerical results.

In Figs. 4–6, cases of a higher F are shown for different values of frequency mismatch Δ. The width of this area is significantly larger from that of Figs. 1–3, as a result of higher F. Electrons with initial actions $J>J_0$ can move to areas of significantly smaller actions $J<J_0$, after undergoing a change of the direction of rotation in the frame of the rf field and evolve in ζ with an almost constant J after a transition length. This transition from a high action value to a lower one is the essential mechanism of efficient gyrotron operation, and is strongly nonuniform in the electron initial angle. The chaotic dependence on the initial angle has also been studied in terms of the Lyapunov exponents, measuring the divergence of nearby electron trajectories, in Ref. 13, where the action reduction accompanied with inversion of the rotation direction has also been shown. The central action value of the area of strong interaction is determined by the frequency mismatch as shown in Figs. 4–6. Specific values

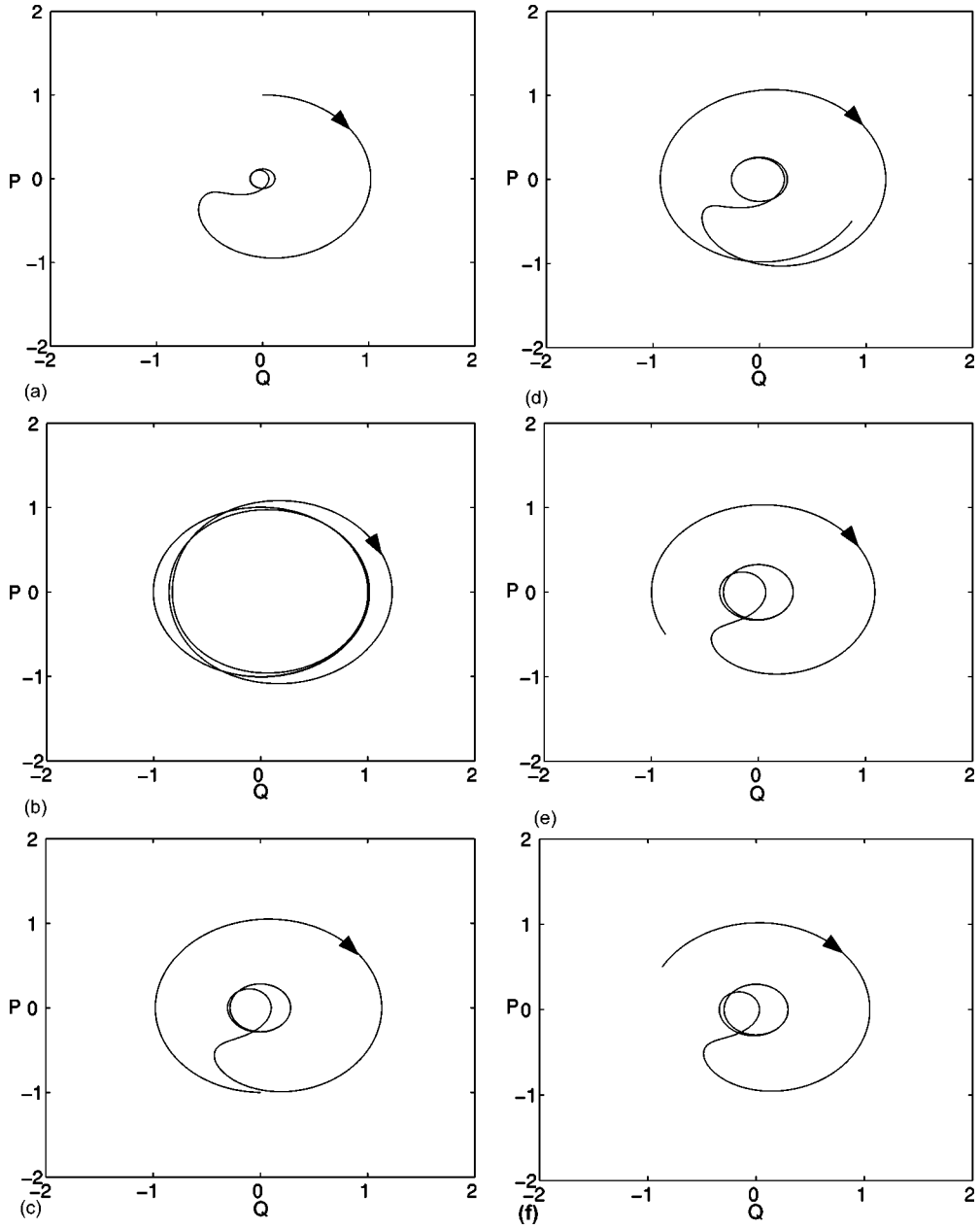

FIG. 9. Phase space trajectories for the same parameter set as in Fig. 8 for initial action value $J=0.5$ and angles $\theta=0$ (a), $2\pi/6$ (b), $4\pi/6$ (c), $6\pi/6$ (d), $8\pi/6$ (e), $10\pi/6$ (f).

of Δ combined with appropriate values of F and μ can result in lower boundaries of the action, under which an initially large action cannot be reduced. The related upper and lower bounds for J are of practical importance for gyrotron operation since estimation of the limits of energy (action) distribution of electrons after their interaction with the rf field in the resonator is a prerequisite for optimizing depressed collectors. Moreover, it can be shown that for certain parameter choices, the initial action of interest can be smaller than J_0, resulting in action increasing for electrons with specific initial angles, and reversing the operation of a gyrotron.

In Fig. 7, the case of $F=0.1$ is shown and Fig. 8 corresponds in the optimum set of parameters $F=0.125$, $\mu=17$, and $\Delta=0.5$ resulting in maximum gyrotron efficiency ($n_\perp=0.71$).[12] In both cases the initial action of interest $J=0.5$ is placed at the higher boundary of the strong interaction area, while the lower boundary is very close to $J=0$; these boundaries correspond to persistent KAM surfaces (cylinders) bounding electron motion in the phase space. However, the larger F of Fig. 8 results in greater portion of transitions of a set of electrons with initial angles distributed uniformly in $[0\ 2\pi)$ and consequently higher efficiency. A few phase space trajectories are shown in Fig. 9, where the critical dependency of the transition to lower action values on the initial angle, as well as the inversion of the direction of rotation are shown. In Figs. 7 and 8, it is shown that the analytical results are in satisfactory agreement with the numerical ones, even for cases of relatively large perturbations.

The approximate constant of the motion given in Eqs. (29) and (30) can be used in order to estimate the width of

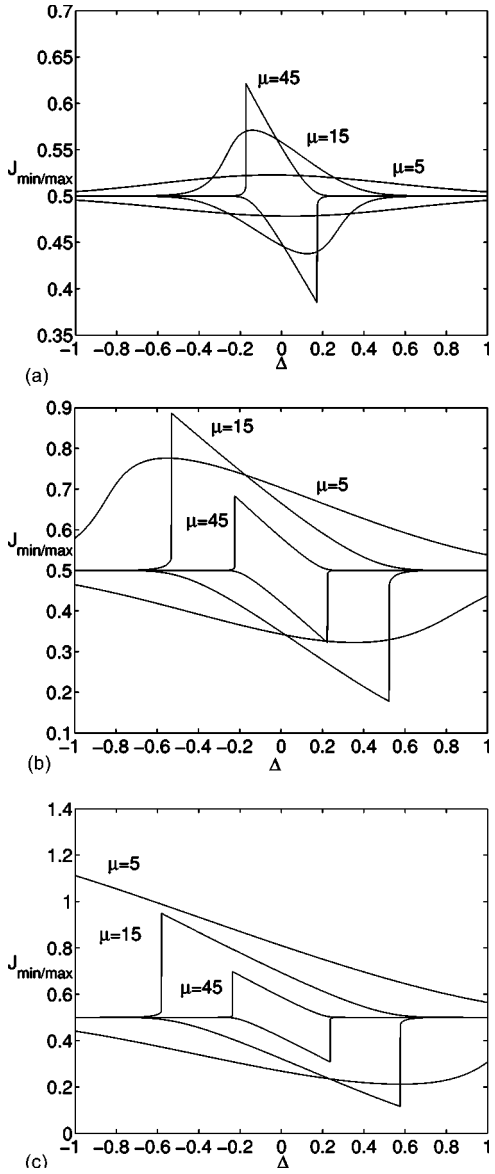

FIG. 10. Upper and lower bounds of electron rest energies as functions of Δ and μ, for $F=0.005$ (a), $F=0.05$ (b), and $F=0.1$ (c).

the energy spectrum of the electrons in terms of the maximum and minimum action. For simplicity of the resulting expression, we assume that electrons with $J_i=0.5$ enter at $\zeta=-\infty$ and leave the cavity at $\zeta=+\infty$ with $J=J_o$, so that Eqs. (29) and (30) result in the following equations for the maximum and minimum of the output action value:

$$J_o \pm \mu F \sqrt{\frac{\pi J_o}{2}} e^{-[(2J_o+\Delta-1)\mu/4]^2} = 0.5. \tag{32}$$

Thus, the action (energy) value range of J_o can be easily obtained as a function of the parameters F, Δ, and μ from the (numerical) solutions of these equations, as shown in Fig. 10. The value range of the frequency mismatch, for which electron action (energy) variation occurs is shown for several values of F and μ. The values of Δ for which a maximum and a minimum action value bifurcates from $J=0.5$, correspond to the case for which $J=0.5$ is placed on the boundary of the strong interaction action area, and resides in a highly distorted KAM curve, as previously shown in the Poincaré surfaces of section. It is remarkable that the calculation of the extrema of the output action reveals two well-known features of the electron dynamics: the assymmetry of the output action spectrum with respect to the line of the initial action value $J=J_i$ and the symmetry with respect to the point $(\Delta,J)=(0,J_i)$. The first is related to the capability of providing nonzero gain and the latter corresponds to the property of inverted operation of the gyrotron resonator for negative frequency mismatches, namely, electron energy increasing. The symmetry is shown to be violated for large deviations from the initial action value. Moreover, the following figures and the underlying Eq. (32) provide a simple tool for obtaining the limiting values of the output electron energy. These values are obtained under the assumption of a fixed rf field. However, they can be utilized as rough estimates providing guidance for the more complex self-consistent model of the electron–rf field interaction and the optimization of the depressed collectors resulting in overall gyrotron efficiency enhancement.

VII. CONCLUSIONS

In this work, electron dynamics in a gyrotron resonator were studied in terms of methods of nonlinear dynamics. The near-integrable system describing electron motion possesses a strongly inhomogeneous phase space structure which is analyzed in terms of Poincaré surfaces of section. The application of a KAM-type theorem for time-aperiodic perturbations of Hamiltonian systems and the canonical perturbation theory led to the analytical construction of approximate local invariants of the flow, which bound electron motion in specific areas of the phase space. Numerical results were shown to confirm the analytically obtained phase space structure in a remarkable agreement. The phase space topology of the unperturbed system (free electron motion) consists of infinite cylinders. Under perturbation (rf field), some of these cylinders are distorted or even destroyed in specific areas of the phase space and electron momentum variation occurs. The latter is the essential mechanism for providing gyrotron efficiency. The inhomogeneity of the phase space, containing areas of strong and weak interactions was explained in terms of resonances between the free electron rotation frequencies and the rf field spectrum.

The aforementioned phase space analysis provides useful information and guidelines for efficient gyrotron design and operation. The dimensionless length of the resonator μ and the frequency mismatch Δ is shown to be, respectively, related to the width and the central action value of the phase space area of strong interaction. High efficient gyrotron operation is achieved for parameters for which the normalized electron transverse momentum (action value $J=0.5$) is just below the upper boundary of the strong interaction area. Finally, knowledge of the boundaries of the electron motion provided through robust (slightly distorted) KAM surfaces is useful preliminary information for practical optimization of depressed collectors using well-known codes (see Ref. 14, and references therein).

ACKNOWLEDGMENTS

This work was supported in part by the European Fusion Programme (EURATOM) and the Greek General Secretariat of Research and Technology. The sponsors do not bear any responsibility for the contents in this work.

APPENDIX: INTEGRAL CALCULATION

The calculation of integral (28) is quite similar to the integral involved in the plasma dispersion relation. The integrand has a simple real pole at $\Omega=-\omega_\theta$, and the contour of integration in the complex plane is deformed in order to bypass the real pole in a counterclockwise direction, so that the integral can be written in the following form:

$$I_0=\frac{1}{2\pi}\left(P\int_{-\infty}^{+\infty}\frac{\mathbb{F}(\Omega)}{\Omega+\omega_\theta}\exp(i\Omega\zeta)d\Omega+i\pi\mathbb{F}(-\omega_\theta)\times\exp(-i\omega_\theta\zeta)\right) \tag{A1}$$

with P denoting the Cauchy principal value of the integral and the second term taking into account the contribution of the real pole. Identifying the first term as an inverse Fourier transform and using the frequency shift and integration properties of the Fourier transform, we have

$$I_0=\exp(-i\omega_\theta\zeta)\int_{-\infty}^{\zeta}f(t)\exp(i\omega_\theta t)dt. \tag{A2}$$

[1] G. G. Denisov, "Megawatt gyrotrons for fusion research. State of the art and trends of development," in *Strong Microwaves in Plasmas*, Proceedings of the International Workshop, Nizhny Novgorod, Russia, 1–9 August 2002, edited by A. G. Litvak (Institute of Applied Physics, Nizhny Novgorod, 2003), p. 29.
[2] G. Dammertz, S. Alberti, A. Arnold, E. Borie, V. Erckmann, G. Gantenbein, E. Giguet, R. Heidinger, J. P. Hogge, S. Illy, W. Kasparek, K. Koppenburg, M. Kuntze, H. P. Laqua, G. LeCloarec, Y. LeGoff, W. Leonhardt, C. Lievin, R. Magne, G. Michel, G. Mueller, G. Neffe, B. Piosczyk, M. Schmid, K. Schwoerer, M. K. Thumm, and M. Q. Tran, IEEE Trans. Plasma Sci. **30**, 808 (2002).
[3] B. Piosczyk, G. Dammertz, O. Dumbrajs, O. Drumm, S. Illy, J. Jin, and M. Thumm, IEEE Trans. Plasma Sci. **32**, 413 (2004).
[4] T. Idehara, S. Mitsudo, R. Pavlichenko, I. Ogawa, D. Wagner, and M. Thumm, "Development of submillimeter wave gyrotron FU series," in *Strong Microwaves in Plasmas*, Proceedings of the International Workshop, Nizhny Novgorod, Russia, 1–9 August 2002, edited by A. G. Litvak (Institute of Applied Physics, Nizhny Novgorod, 2003), p. 116.
[5] G. S. Nusinovich, *Introduction to the Physics of Gyrotrons* (The Johns Hopkins University Press, Baltimore, 2004).
[6] M. I. Airila and O. Dumbrajs, Nucl. Fusion **43**, 1446 (2003).
[7] A. J. Lichtenberg and M. A. Lieberman, *Regular and Chaotic Dynamics* (Springer, New York, 1992).
[8] M. I. Airila, O. Dumbrajs, A. Reinfelds, and D. Teychenne, Int. J. Infrared Millim. Waves **21**, 1759 (2000).
[9] O. Dumbrajs and D. Teychenne, J. Commun. Technol. Electron. **47**, 1364 (2002).
[10] G. S. Nusinovich, R. Ngogang, T. M. Antonsen, Jr., and V. L. Granatstein, Phys. Rev. Lett. **93**, 055101 (2004).
[11] T. V. Borodachyova, A. L. Goldenberg, and V. N. Manuilov, *Gyrotrons* (Institute of Applied Physics, Gorky, 1989), p. 161.
[12] G. S. Nusinovich and R. E. Erm, Electron. Tekh. Ser. 1 Elekronika SVCH **8**, 55 (1972).
[13] O. Dumbrajs, R. Meyer-Spasche, and A. Reinfelds, IEEE Trans. Plasma Sci. **26**, 846 (1998).
[14] C. Ling, B. Piosczyk, and M. K. Thumm, IEEE Trans. Plasma Sci. **28**, 606 (2000).